Analyst

Accepted Manuscript

This article can be cited before page numbers have been issued, to do this please use: W. H. Kim, J. U. Lee, S. Song, S. Kim, Y. J. Choi and S. J. Sim, *Analyst*, 2019, DOI: 10.1039/C8AN01745J.

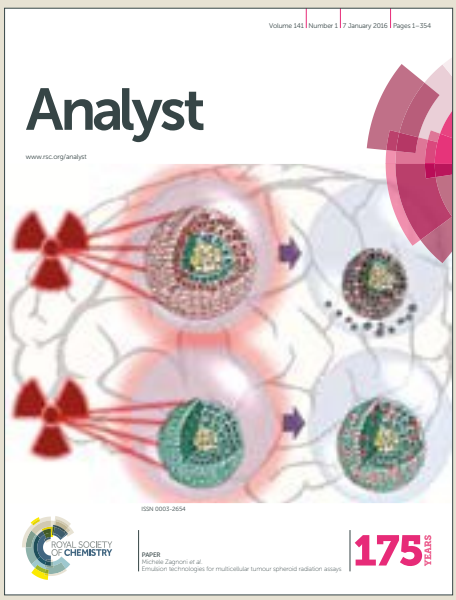

This is an Accepted Manuscript, which has been through the Royal Society of Chemistry peer review process and has been accepted for publication.

Accepted Manuscripts are published online shortly after acceptance, before technical editing, formatting and proof reading. Using this free service, authors can make their results available to the community, in citable form, before we publish the edited article. We will replace this Accepted Manuscript with the edited and formatted Advance Article as soon as it is available.

You can find more information about Accepted Manuscripts in the author guidelines.

Please note that technical editing may introduce minor changes to the text and/or graphics, which may alter content. The journal's standard Terms & Conditions and the ethical guidelines, outlined in our author and reviewer resource centre, still apply. In no event shall the Royal Society of Chemistry be held responsible for any errors or omissions in this Accepted Manuscript or any consequences arising from the use of any information it contains.

ROYAL SOCIETY OF CHEMISTRY

rsc.li/analyst

Analyst

View Article Online
DOI: 10.1039/C8AN01745J

PAPER

Label-free, ultra-highly sensitive and multiplexed SERS nanoplasmonic biosensor for miRNA detection using head-flocked gold nanopillar †

Received 00th January 20xx,
Accepted 00th January 20xx

DOI: 10.1039/x0xx00000x

www.rsc.org/

Woo Hyun Kim,‡[a] Jong Uk Lee,‡[a] Sojin Song,[a] Soohyun Kim,[a] Young Jae Choi,[a] and Sang Jun Sim*[a]

Cell-free micro-ribonucleic acids (cf-miRNAs) regulate most of the human genes by control the mRNA translation and have been considered as the most promising biomarkers for cancer diagnosis and prognosis. Due to their low abundance, short length, and similar sequences, an attractive approach that is ultrasensitive and label-free is hugely demanded. Herein, we develop a label-free, ultra-high sensitivity and selectivity multiplex miRNA using surface-enhanced Raman scattering to detect cancer-associated miRNAs with head-flocked gold nanopillars as a substrate. Using complementary DNA probe platform and an ultra-high sensitivity SERS based biosensor, we achieved high selectivity in targeting miRNAs with extremely low detection limits, without any chemical or enzymatic reactions and evaluated the correlation between the miRNA expression level and the Raman signal intensity. A reproducible SERS signal is monitored via uniformly fabricated elastic head-flocked gold nanopillars through mapping method. This system supports the detection of cell-free miRNAs in blood, which are utilized and quantified as biomarkers to diagnose and provide a prognosis for cancers and intractable diseases. In the foreseeable future, this advanced label-free miRNA detection system is highly promising for a less tumor-invasive biopsy for the early diagnosis and prognosis of cancer.

1. Introduction

Cancer is one of the most perilous diseases and the second leading cause of patient mortality, with globally 1 in 6 deaths. Mortality due to cancer is expected to increase by approximately 70% over the next two decades.[1] Accordingly, the need to improve cancer diagnosis techniques is increasing. Detection of cancer in the early or metastatic stages is an essential prerequisite for the effective diagnosis and treatment of cancer. However, it is difficult to collect sufficiently large sample amounts at the early stages of cancer and conventional biomarkers are often only observed at the disease's onset. Doctors and researchers have been investigating improved bio-informative biomarkers for more effective diagnoses throughout the last decade.[2]

Normally, many molecular pathways in cancer cells are influenced both by canonical protein-coding genes and by non-coding genes.[2] One class of non-coding gene is microRNA, which is small (20–24 nucleotides) and suppresses or promotes gene expression in the RNA-induced silencing complex (RISC).[3] Moreover, miRNAs indicate the initial phase of cancer and the tumour stage's progression in tissue and blood through different expression levels.[4,5] In particular, recent studies have shown that miRNAs can be released from cells and secreted in human biofluids, including blood serum, plasma, urine and saliva. This release can occur both in response to the apoptosis and necrosis of cancer cells and as an active release; furthermore, miRNAs contain specific cancer information and have high stability in both plasma and serum.[6] These miRNAs, called cell-free miRNAs, can act as noteworthy biomarkers in cancer diagnoses.[7] Some studies have demonstrated that the cancer-related overexpression of several miRNAs is further increased in the metastatic state of some cancers including glioblastoma, breast cancer, lung cancer and chronic lymphocytic leukaemia.[8] Hence, an advanced detection system that identifies the miRNA expression level in a blood sample is possible.

[a] Department of Chemical and Biological Engineering, Korea University, Seoul 02841 (South Korea), Email: simsj@korea.ac.kr

† †Electronic Supplementary Information (ESI) available: [details of any supplementary information available should be included here]. See DOI: 10.1039/x0xx00000x

‡ These authors contributed equally to this work

View Article Online
DOI: 10.1039/C8AN01745J

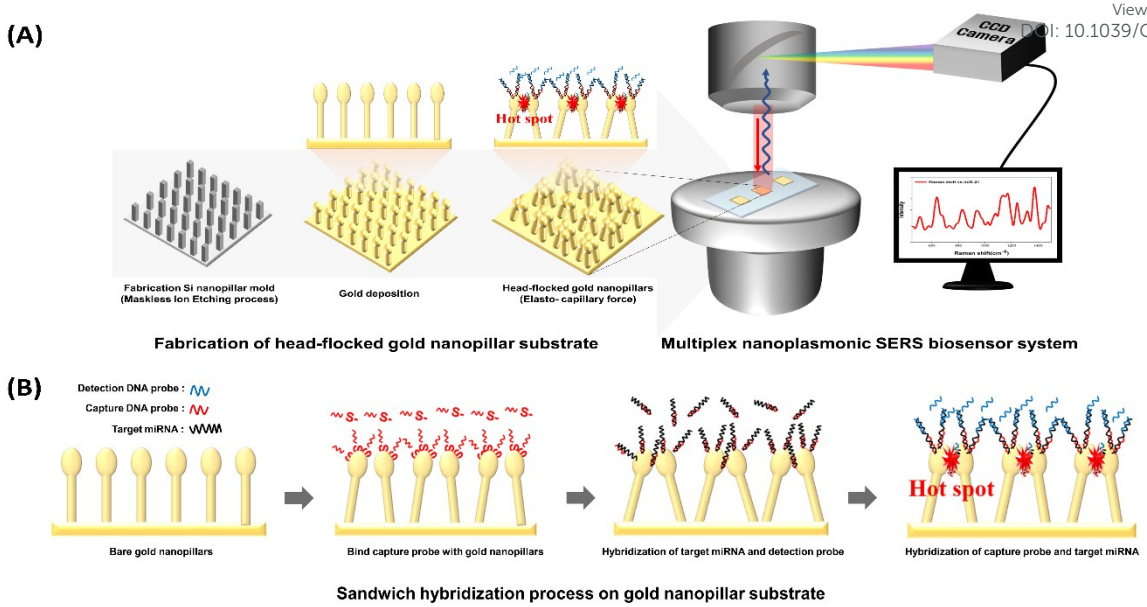

Fig. 1 A schematic of the multiplex SERS nanoplasmonic biosensor using head-flocked gold nanopillars for label-free detection of miRNA. (A) Fabrication of head-flocked gold nanopillar substrate and multiplex nanoplasmonic SERS biosensor system, (B) Sandwich hybridization process for miRNA detection.

Researchers have developed various methods for detecting the miRNA expression level. Northern blotting is the most standard method but is a time-consuming process with some contamination risk. Although microarrays can simultaneously detect hundreds of miRNAs, probe fixation and labelling are inevitable. Real-time polymerase chain reaction (RT-PCR) has high sensitivity, but this method also has a weak point that results from the cost of materials used in the cDNA synthesis process. Quantitative RT-PCR (qRT-PCR) has been introduced as an option for the quantitative detection of target miRNA, but this method also requires several complex pre-processing steps and further labelling steps. In addition to these drawbacks, fluorescence is sensitive to quenching effects from the excitation light or environmental factors, and the sample's autofluorescence or background signal commonly restricts fluorescent analysis.[9] In terms of molecular biology, the small size, the significant sequence homologies among the miRNA family group and the low expression levels of miRNA restrict the quantitative analysis of miRNA.[10] There is a high demand for new strategies that will detect miRNA quantitatively and overcome previous methods' disadvantages.

Surface-enhanced Raman scattering (SERS) is a highly sensitive and selective technique that is chemically specific and does not require labels to detect miRNA. The vibration fingerprints produced by SERS can show molecular and structural information about biological samples.[11] Compared to conventional methods, the SERS-based detection system is less time-consuming due to its streamlined sample preparation procedure;[12] therefore, SERS has the potential to become a powerful tool for miRNA detection. Nevertheless, the quantification of miRNA based on the SERS system has limitations that have been obstructed by the poor uniformity and reproducibility of SERS substrates such as metal nanoparticles, metal nanofilms, and others. In addition, specific binding and fluctuations in signal intensities impede the development of SERS-based quantitative analysis.[13]

Herein, we sought to overcome the limitations described by developing a label-free, ultra-sensitive, highly selective SERS-based detection platform to detect miRNAs related to cancer metastasis in patient-mimicking serum. We chose three types of specific target miRNAs (miR–10b, miR–21 and miR–373) that are well-known to be closely related to cancer metastasis, invasion and apoptosis.[8,14,15] We fabricated a head-flocked gold nanopillar(hfAuNP) for the SERS substrate that resulted in the generation of the head-flocked effect which produces the electromagnetic enhancement of the Raman scattering by forming strong hot spot regions.[16] We confirmed different finger print peaks depending on each target miRNA sequences with the DNA probes for sandwich hybridization. We confirmed a Raman signal reproducibility of the hfAuNP substrate through Raman mapping method which was used to verify the Raman signal trends in large area substrate. Thus, this SERS-based label-free miRNA detection platform demonstrates high selectivity in targeting miRNAs with distinction in single nucleotide level. Its sensitivity was at fM levels without any chemical or enzymatic reactions. Consequently, the near-perfect classification of miRNA finger print peaks was achieved, leading to quantitative (10 fM–1 μM) and multiplex detection of the target miRNAs. Therefore, the developed multiplex SERS nanoplasmonic biosensor offers the combination of high selectivity with high sensitivity, without additional labelling, and thus has the potential to provide ideal features for an optimal miRNA sensing method. We predict that the system will not only be able to detect cancer, but also to diagnose and predict the prognosis of intractable diseases and elucidate the therapeutic effect of anticancer drugs.

View Article Online
DOI: 10.1039/C8AN01715J

2. Experimental

2.1. Materials

BOROFLOAT® 33 was purchased from Schott Korea (Korea). The Au pellet (Ø 3×3 h, 99.99 %) was purchased from Sin-woo Metal (Korea). Human serum, sodium sulfate anhydrous (Na_2SO_4), sodium chloride ($NaCl_2$), trisodium citrate, hydrochloric acid (HCl, 37 wt% in water), 6-mercapto-1-hexanol (MCH, 97 %), 1, 4-dithiothreitol (DTT), and ethyl acetate (anhydrous 99.8 %) were purchased from Sigma Aldrich (Korea). Ambion® nuclease-free water was purchased from Thermo Fisher Scientific (Korea). DNA LoBind (1.5 mL) tubes were purchased from Eppendorf. Ultra-pure water (18.2 mΩ cm^{-1}) was used to prepare all solutions. All DNA probes and target miRNA sequences were purchased from Bioneer (Korea).

2.2. Synthesis of DNA probe for hybridization with target miRNAs

DNA probes were designed with two different parts, including capture and detection. To confirm the SERS signal transition with each step of hybridization between the DNA probe and the target miRNA, we separated the roles of the DNA probe. The DNA capture probe plays the role of a conjugation DNA probe with the head-flocked gold nanopillar structure. The DNA detection probe acts to identify complete hybridization. To determine the sequence of each DNA probe, we considered the G–C content ratio ((40–60) %), with overlap of three or more bases between different DNA probes, and the T_m for regulation of nonspecific hybridization and for the optimal conditions of hybridization. Using the OligoAnalyzer® Tool from Integrated DNA Technologies (IDT), Table. 1 confirms the G–C content ratio, T_m values, length, self-dimer and hetero-dimer of each probe. For the conjugation DNA capture probe with gold nanopillars, we modified the thiol group at the 5 '- end of the capture probe from Bioneer (Korea).

Table. 1 Characterization of DNA probes

Probe	Length(nt)	C-G contents (%)	Tm(℃)
miR–10b capture	12	41.7	31.8
miR–10b detection	11	45.5	30.8
miR–21 capture	11	36.4	24.3
miR–21 detection	11	36.4	29.1
miR–373 capture	12	50	37.5
miR–373 detection	11	45.5	34.2

2.3. Fabrication of head-flocked gold nanopillar structure

For head-flocked gold nanopillar fabrication, we fabricated an elastic silicon nanopillar mold, using a maskless reactive ion plasma etching (RIE) process.[17] The maskless RIE process is a dry etching method that uses chemically reactive plasma without a film mask to generate the nanopillar shape.[17] Four-inch p-type silicon wafers were used, and etching was performed using a Plasma Lab100 instrument from Oxford Instruments (Micro/Nano Fab Center, Korea Institute of Science and Technology) with the following parameters: SF_6:O_2 flow ratio (1.12), platen power (110 W), chamber pressure (36 mTorr) and rate (3 nm/s). To avoid effects on the subsequent SERS spectrum, the maskless reactive ion etching process was followed by physical removal of remnants by exposure to oxygen plasma. To metalize the elastic silicon nanopillar mold, gold was coated on the elastic silicon nanopillar through an electron beam evaporation process. In this process, the metallization deposited more gold on the head of the elastic silicon nanopillar structure. Head-flocking was observed during liquid sample treatment and was confirmed by SEM (Fig. 2 and Fig. S1 ESI†). Additionally, we fabricated multi-cast slide glass using silicate glass (BOROFLOAT® 33). Since this cast was designed by the AutoCAD program and the number and size of the cast could be controlled, it became the basis of the multiplex system. Next, we etched the glass using Quartz, Pyrex Vertical/Slant glass etching method. We loaded each SERS substrate on the multi-cast slide glass, and sequentially measured SERS signal of each SERS substrate by one slide glass.

2.4. Preparation of DNA probe conjugated with the head-flocked gold nanopillar substrate and hybridization of DNA probe and target miRNA

For complete conjugation of the DNA probe with the head-flocked gold nanopillar, we activated thiol group in the capture probe using DTT, which is a reducing agent, with the formation of a disulfide bond by the typical 2 serial thiol-disulfide interchange reaction. Since the modified capture probe had a disulfide bond at the 5' end, DTT that could break the disulfide bond was used. Capture probe solution (10 μM) was added to the conjugation buffer containing Na_2SO_4 (30 mM) and nuclease–free water of pH ~7. The head-flocked gold nanopillar substrate was incubated in capture probe solution for 12 h at 30 °C. After incubation, the head-flocked gold nanopillar substrate was washed with DI water and flushed with N_2. Self-assembled monolayers consisting of MCH play an important role as spacers that prevent the nonspecific binding that occurs when DNA strands bind to gold or silver surfaces.[18] MCH (10 μM) solution was added to the conjugation buffer. The head-flocked gold nanopillar substrate that had been treated with the capture probe was incubated in MCH solution for 3 h at room temperature and was then washed by washing buffer, including 2× saline-sodium citrate (SSC) buffer and 0.2 % sodium dodecyl sulfate (SDS). After the previous step, the substrate was completely washed with DI water and flushed with N_2. For hybridization between the capture probe and the target miRNA, we prepared patient-mimicking serum samples which were composed of human serum (Sigma Aldrich) spiked with synthesized target miRNAs (Bioneer) ranging from 100 aM to 1 μM. The head-flocked gold nanopillar substrate was incubated for 12h at 30 °C, followed by washing out unhybridized target miRNAs with DI water and N_2 drying. To hybridize the detection probe with miRNA, we prepared hybridization buffer consisting of 2× SSC, nuclease-free water, and the detection probe (10 μM) at 30 °C for 6 h, followed by washing out with DI water and N_2 drying.

2.5. Detection of miRNA and relative quantitative analysis based on SERS

After sampling DNA probes and miRNAs on the head-flocked gold nanopillar substrate, these gold nanopillar chips were directly loaded into multi-cast slide glass for multiplex measurement. Using silicone gel, the head-flocked gold nanopillar chips were attached to the multi-cast slide glass loading areas. The SERS signals of the DNA probe and miRNA were measured using customized Raman microscopy from NOST (Korea). The excitation laser (785 nm) was

focused through the 100× air objective (TU Plan ELWD 100×, Nikon, 0.6 NA, 0.56 mm WD) of the upright microscope (Eclipse Ni-U, Nikon). The direction of light polarization was controlled by a linear polarizer (PRM 1/ M, Thorlabs). The intensity of the laser was set at 10.67 mW using a digital power meter (PM100, Thorlabs). To obtain the optimal condition for SERS measurement, we used various experimental conditions of exposure time, confocal slit, accumulation number, and ND filter ratio. The exposure time was 0.5 s, the confocal slit size was 120 µm, the accumulation number was 30, and the ND filter ratio was 16 %. The Raman signal from miRNAs was processed through a spectrograph (Interchangeable grating aberration free spectrograph, FEX) and a CCD camera (Newton 920, Andor Technology). SERS mapping data was measured by using the 785 nm laser line with 10.67mW power and a 50× objective lens. The exposure time and ND filter ratio were 0.5 s and 16 % respectively. The slit size 120 µm and detecting spectra region 600–1800 cm^{-1}. The mapping area was 50 × 50 μm^2 with step size of 2 µm. Data analysis was conducted with SpectroLab 2.5 from NOST (Korea) and Origin 8 software.

2.6 Cell culture and Quantitative Real Time Polymerase Chain Reaction (qRT-PCR) analysis of target miRNAs

Human breast MCF-7 cell line was obtained from the American Type Culture Collection (ATCC) (Manassas, VA, USA). It was cultured at 37 °C in RPMI 1640 medium supplied with 4 mg/mL insulin (human recombinant, zinc solution; Life Technologies, Grand Island, NY, USA), 10% fatal bovine serum, 100 U/mL of penicillin, 100 mg/mL streptomycin, and 2 mM L-glutamine under 5% CO_2 condition. The total RNA including miRNA was extracted from the cells using a RNeasy Mini Kit (Qiagen, Valencia, CA, USA). The concentrations of RNAs were measured with a spectrophotometer by the absorbance at 260 nm. qRT-PCR was conducted for the quantification of miRNA using TaqMan miRNA reverse transcription kit (Biosystems, Korea) with Biosystems StepOnePlus real-time PCR system.

3. Results and discussion

3.1. Fabrication of the SERS nanoplasmonic biosensor

For the fabrication of the SERS nanoplasmonic biosensor, we produced a head-flocked gold nanopillar(hfAuNP) SERS substrate (4 × 4 mm) (Fig. 1) and confirmed its effects using a scanning electron microscopy (SEM) image (Fig. 2A). We made a Si nanopillar structure via a maskless dry etching process[19] and deposited gold on the silicon nanopillar via an electron beam evaporation process.[20] This structure was composed of uniform and mountaintop-shaped gold nanopillars of average height 800 nm and average width 200 nm. Subsequently, the gold nanopillars formed "flock" structures under exposure to liquid sample flowing through a part of the nanopillar structure (Fig. 2B). This phenomenon was named the "head-flocking" effect. This effect occurred due to the elastocapillary force pulling the nanopillars together and reducing the gap distance between the nanopillars to a nanometre-size gap.[11,21,22] Head-flocking effect enhanced the electromagnetic field by plasmonic coupling in localized surface plasmon resonance (LSPR).[23,24] Therefore, the hfAuNP SERS substrate generated

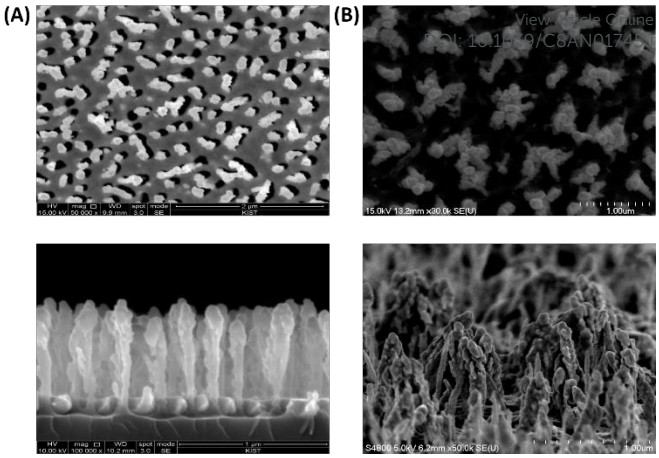

Fig. 2 Fabrication of the head-flocked gold nanopillar SERS substrate: (A) SEM images of the pure structure of the gold nanopillars before sample treatment and (B) SEM images of the head-flocked gold nanopillar SERS substrate after sample treatment

sufficient hotspots for strong SERS signals in large areas.[25,26] As shown in Fig. S1 ESI†, the hfAuNP s exist at a high density over a wide area in the SEM image. Moreover, this substrate has a uniform head-flock structure and strong signal intensity formed over the entire area through Raman mapping to confirm the signal (Fig. S2 ESI†). A Raman signal's reproducibility is generally determined by the uniformity of the structure (or the structural uniformity of the substrate) and dense SERS hotspots distribution on the substrate.[26] Thus, the hfAuNP SERS substrate was capable of detecting the analyte with both high sensitivity and signal reproducibility in large area. In addition, the stability of the SERS nanoplasmonic biosensor was confirmed by continuously measuring the intensity of fingerprint peak being stored in human serum at 30℃ for 9 days (interval 2 days). Fig. S3 ESI† shows plot Raman intensity at 1167 cm^{-1} (I_{1167}) as a relationship of storage time indicating a very small variation (~1.19%) of I_{1176}. This result shows that the performance of the SERS nanoplasmonic biosensor very stable even after one week's storage.

We detected target miRNAs using the hfAuNP substrate by synthesizing detection probes and capture probes that have a complementary sequence to the target miRNAs (Table S1 ESI†). The miRNA detection system's development was extremely difficult because many miRNA have similar sequences, family groups, and single-nucleotide mismatch variations.[27] The sandwich hybridization method is commonly used to increase the stability of hybridization affinity during the hybridization process and it may be useful since the sample is kept in solution throughout the process in a crude sample (blood, cell lysate, serum, etc.).[27] Recently, research of miRNA detection also was used to sandwich hybridization method.[28, 29] The DNA capture probe adhered to the surface of the hfAuNP structure via disulphide bonding. The DNA detection probe played a role in distinguishing the fingerprint peak of target miRNAs through the hybridization process. To hinder the nonspecific hybridization between DNA probes and miRNAs, the probe sequences were designed to have fewer than three identical consecutive nucleotides. Moreover, to

View Article Online
DOI: 10.1039/C8AN01745J

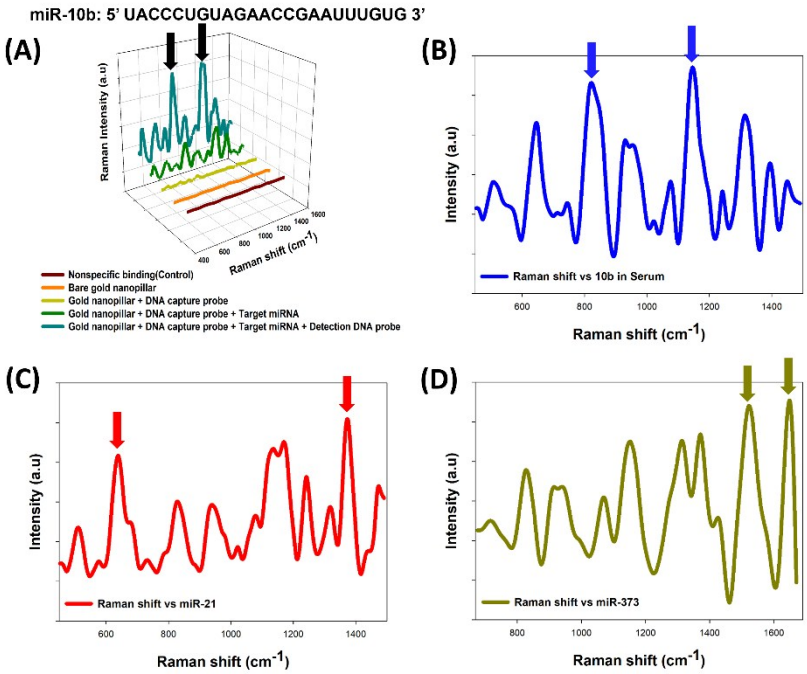

Fig. 3 SERS measurement of the signal transition in process and the miRNA fingerprint peak: (A) Signal transition of miR–10b in four steps, including bare gold nanopillars, gold nanopillars conjugated with the DNA capture probe, the DNA capture probe hybridized with the target miR–10b, and the target miR–10b hybridized with the DNA detection probe, (B) the miR–10b Raman spectra at 100 nM, (C) the miR–21 Raman spectra at 100 nM, and (D) the miR–373 Raman spectra at 100 nM in the optimal condition.

induce hybridization between DNA probes and target miRNAs at 30°C, probe sequences were designed with 40–60% GC content to increase the melting temperature (T_m) (Table 1). The SERS nanoplasmonic biosensor is now ready to detect target miRNAs for multiplex biosensing based on a successful hybridization process on the surface of the hfAuNP SERS substrate.

3.2. Discrimination of miRNA detection with the label-free SERS nanoplasmonic biosensor.

We used the label-free SERS nanoplasmonic biosensor to discriminate between target miRNAs (miR–10b, miR–21, and miR–373) by performing SERS signal measurement according to the hybridization process under optimal conditions. As shown in Fig. 3A, there was no specific SERS signal spectrum when we confirmed in the untreated state of gold nanopillar substrate (as illustrated by the Orange line in Fig. 3A). The metal substrate is composed of monoatomic molecules with no chemical or structural vibrations, and the original Raman signal is thus not generated with the SERS mechanism. Instead, the metal substrate is used for electron donors to engender SERS.[30] We measured the SERS signal of the gold nanopillar conjugated with a single-stranded DNA capture probe (as illustrated by the olive-green line in Fig. 3A). The results presented no significant difference in SERS signal spectra before and after the conjugation of capture probes since the chemical bonds were insufficient for signal variation.[31,32] However, after the hybridization of target miRNAs with DNA probes, the signal intensity was amplified 10–20 fold (green and light sea green line, Fig. 3A) the intensity was achieved with the bare hfAuNP. This amplification occurred because the number of hfAuNP structures were increased by the elastocapillary force for the process of sample treatment. In addition, base parings and chemical bondings (NH_2, CH_3, C_6H and others) were increased by hybridization between the target miRNA and DNA probes.[33] These results indicate that the hybridization process was successfully conducted on the SERS nanoplasmonic biosensor and that this system has high-intensity SERS signals via label-free analysis for detecting miRNAs. The archetypal Raman vibrational frequency of a pure nucleotide can be defined by many of its components, including vibrations of the base during ring breathing and chemical stretching, or the sequential order of temperatures and DNA and RNA sequences and hybridizations.[33–35] Based on these properties and the literature, we detected three types of target miRNA (miR–10b, miR–21 and miR–373) that have different fingerprint peaks depending on various conditions, including the DNA and RNA sequences, A:C:G:T ratios, the orientation of DNA and RNA on the surface of the SERS substrate and DNA hybridization (Table 2 and S1 ESI†).[36–38]

Table. 2 Raman frequencies of vibrational Modes at fingerprint peak of chemical bonds and bases with the head-flocked gold nanopillar

Raman shift (cm^{-1})	Assignments
640	A, G, ring breathing
825	U, T ring breathing
1167	(C_8H, N_{10}–H_{11}), (C_4–N_9, N_3–C_4, C_6–N_{10})
1376	CH_3, C_6H deformation
1521	A, G
1650	T, C and NH_2

View Article Online
DOI: 10.1039/C8AN01745J

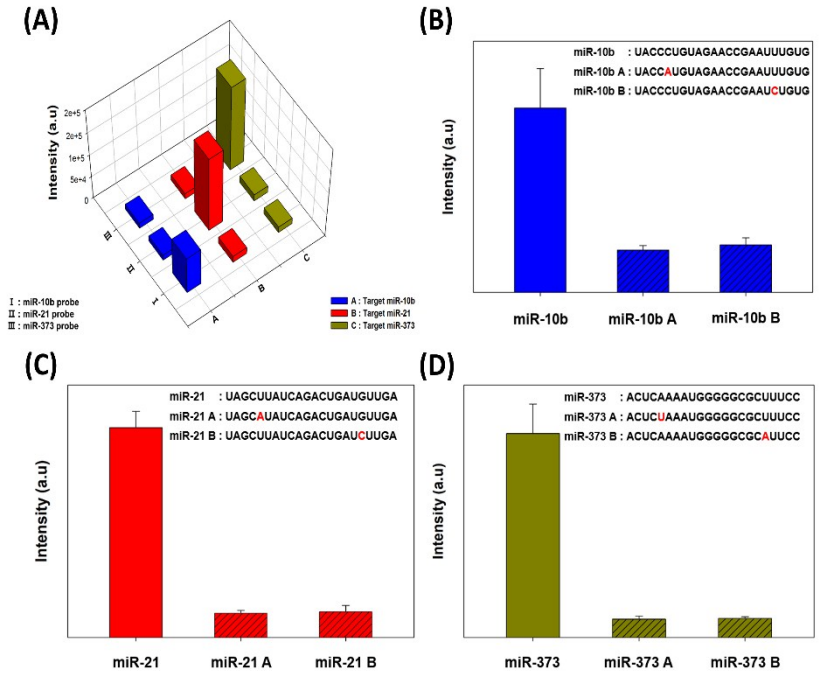

Fig. 4 Raman intensity of the label-free SERS-based multiplex plasmonic biosensor for the evaluation of nonspecific binding to miR–10b, miR–21, and miR–373 at the main peak : (A) Detection of unspecific hybridization between DNA probes and target miRNA (miR–10b, miR–21, miR–373) describing 3D horizontal graph at main fingerprint peak and (B) Plots of miR–10b main fingerprint peak (1167 cm^{-1}) intensity with miR–10b and single nucleotide mismatch samples at 100nM , (C) Plots of miR–21 main fingerprint peak (1376 cm^{-1}) intensity with miR–21 and single nucleotide mismatch samples at 100 nM, (D) Plots of miR–373 main fingerprint peak (1650 cm^{-1}) intensity with miR–373 and single nucleotide mismatch samples at 100 nM.

As shown in Fig. 3B and Table 2, we measured the fingerprint peaks of miR–10b at 825 and 1,167 cm^{-1}. These peaks were assigned to the in-ring breathing of cytosine and the C–C, C–N and N–H stretching of the DNA and RNA backbone.[33,39] The miR–21 fingerprint peaks at 640 and 1,376 cm^{-1} were assigned to the in-ring breathing of adenine and guanine and the CH_3 and C_6H deformation (Fig. 3C).[33,40] The fingerprint peaks of miR–373 were measured at 1,521 and 1,650 cm^{-1}. In Fig. 3D, the Raman spectrum is affected by cytosine and guanine molecules, which give rise to adenine and guanine ring breathing (1,521 cm^{-1}), and cytosine and NH_2 stretching modes (1,650 cm^{-1}).[33,34] These results support our label-free SERS nanoplasmonic biosensor's ability to enable the discrimination of target miRNAs with a target-specific SERS fingerprint.

3.3. Selectivity of the multiplex SERS nanoplasmonic biosensor

One major issue of label-free multiplex SERS biosensors is that cross-reactions occur on the sensor surface depending on the increase in the number of target analytes.[41,42] many studies have sought to reduce cross-reactions by developing a multiplex biosensor based on a specific reaction (e.g., antigen/antibody) to identify cross-reactivity. In this study, we developed a multiplex, SERS nanoplasmonic biosensor using a DNA capture/detection probe that has a complementary sequence to target miRNAs (miR–10b, miR–21 and miR–373). These probes can detect their target miRNA through specific binding. However, biofluids consist of many types of target miRNAs, DNA, RNA, protein and high-density lipoprotein, which cause non-complementary binding with the DNA capture/detection probe.[43] Furthermore, more than 24,000 miRNAs exist in blood. Among them, many miRNAs have comparable sequences to each other, and family groups have only a few different bases in the seed region such as the miR–10 family (miR–10a, miR–10b, miR–99a, miR–99b, miR–100 and miR–125).[44] Thus, carefully evaluating the selectivity and non-specific binding of DNA probes to other biomolecules is essential along with single nucleotide mismatch.

We confirmed the selectivity of the multiplex SERS nanoplasmonic biosensor by measuring the Raman spectra using fingerprint peaks for each target miRNA (100 nM) in human serum. The fingerprint peak with the greatest increase in Raman signal intensity for a specific peak in the obtained miRNA spectra was defined as the main peak. The 3D vertical graph in Fig. 4A (main peak) shows the Raman signal intensity of the fingerprint peaks in the multiplex SERS nanoplasmonic biosensor for the independent detection of miR–10b, miR–21 and miR–373. These results indicate negligible nonspecific binding between the target miRNAs and DNA probes in this sensor. Moreover, we synthesized mismatched miRNAs (types A and B) to confirm single nucleotide mismatches. Fig. 4B compares target miR–10b signal intensities at the fingerprint main peak. Likewise, Fig. 4C and 4D compare miR–21 and miR–373. Only perfectly matched target miRNAs had strong signal intensity among the three miRNAs in the patient-mimicking serum at 100 nM. Thus, the multiplex SERS nanoplasmonic

View Article Online
DOI: 10.1039/C8AN01745J

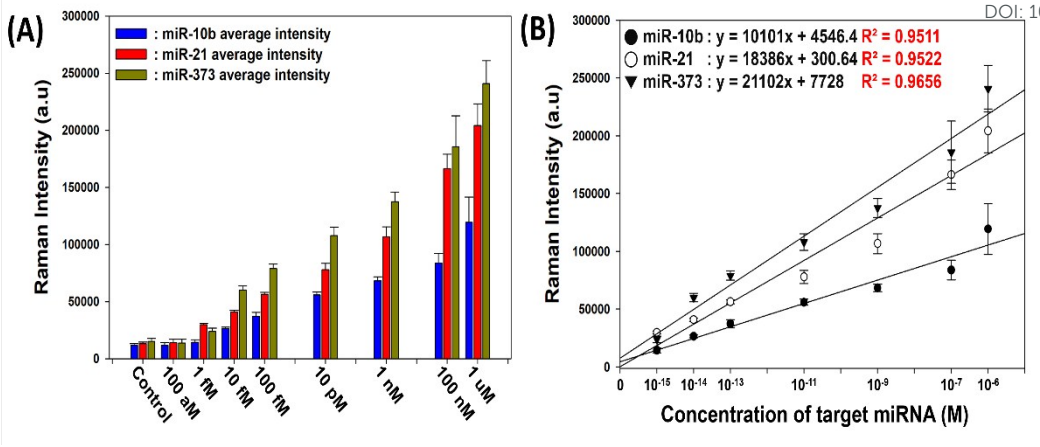

Fig. 5 Detection of miRNAs related to the metastasis state in patient-mimicking serum at the main peak (miR–10b, miR–21, and miR–373) : (A) Average Raman signal intensity (n=20) of each target miRNA concentration, and (B) linear regression of the calibration curve illustrating the relationship between the Raman signal intensity and concentration of target miRNA.

biosensor had high selectivity for the detection of targeted miRNAs at the single-base level.

3.4. Label-free SERS nanoplasmonic biosensor for quantitative analysis

We evaluated the sensitivity of the plasmonic biosensor by performing quantitative analysis of target miRNAs (miR–10b, miR–21 and miR–373) using patient-mimicking serums as model analytes. Under optimal conditions, each target miRNA's detection was conducted using various concentrations of miR–10b, miR–21 and miR–373 from 10^{-1} fM to 10^{9} fM. By analysing the signal intensity increase of the SERS fingerprint peaks based on the concentration of target miRNAs, we confirmed that the increasing Raman signal intensity was highly correlated with the concentration of target miRNAs at fingerprint peaks (Fig. 5A). The increases in SERS intensity indicated a strong logarithmic relationship with miRNA concentration (Fig. 5B). Normally, the coefficient of determination is an important factor in assessing the correlation between dependent and independent variables in statistics; thus, the higher the coefficient of determination, the greater the reliability of the correlation between the two variables. The linear regression equations of the three target miRNAs (main peak) were y = 10101x + 4546.4 (R^2 = 0.9511) for miR–10b, y = 18386x + 30.64 (R^2 = 0.9522) for miR–21 and y = 21102x + 7728 (R^2 = 0.9656) for miR–373. These results indicate that our system clearly provides highly sensitive and label-free quantitative analysis of biomarkers. The biosensor's limit of detection (LOD) values were calculated using the formula LOD = 3*δ/m where δ is the standard deviation of the blank and m is the gradient of the linear regression equation.[24,45] The calculated LOD values for the main peak were 3.53 fM for miR–10b, 2.17 fM for miR–21 and 2.16 fM for miR–373. These results verified both the linear regression equation and the coefficient of determination. Moreover, the comparison of different methods for miRNA detection is

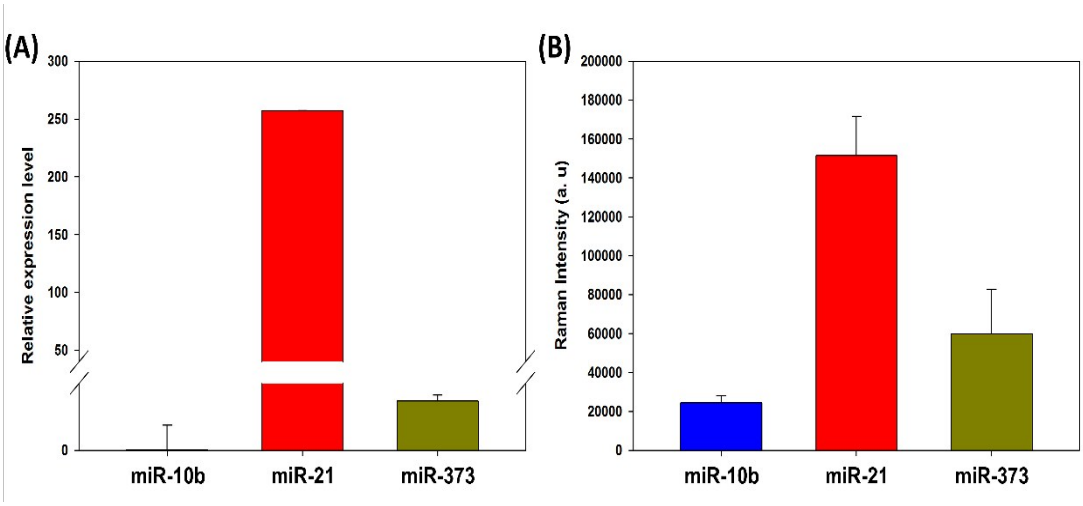

Fig. 6 Analysis of target miRNAs (miR-10b, miR-21, and miR-373) in total RNA extracted from MCF-7 cell line by the SERS nanoplasmonic biosensor and a qRT-PCR kit, respectively. (A) Relative expression level of target miRNAs by qRT-PCR, (B) Raman intensity of target miRNA by the SERS nanoplasmonic biosensor system.

shown in Table. S2. Through this, our sensor system can identify an efficient system for detecting miRNAs in the biofluids.

Finally, to determine whether our SERS nanoplasmonic biosensor could be applied to a real biological sample, we evaluated a testing for target miRNAs in human breast cancer cell lines (MCF-7). The results showed that miR-21 was the most abundantly expressed in MCF-7 cell lines. In contrast, MCF-7 cell lines exhibit the low expression level of miR-373 and miR-10b. These results were in good accordance with previous studies.[14,15,46] The same samples were also analyzed by using qRT-PCR. As shown in Fig. 6, the results indicated by our system were in good accordance with those by qRT-PCR. Therefore, our SERS nanoplasmonic biosensor is practical for miRNA absolute quantification in real samples.

4. Conclusions

In this study, we developed a SERS-based plasmonic biosensor that we used for the label-free multiplex detection of miRNAs; miR–10b, miR–21 and miR–373 were analysed as they are known to be relevant to cancer metastasis. A SERS-based nanoplasmonic biosensor was fabricated with the application of a head-flocked gold nanopillar(hfAuNP) substrate. We designed capture and detection probes complementary to targeted miRNAs for the selective and effective detection of target miRNAs without labels in biofluids through investigation of cross-reaction between target miRNAs and DNA probes in single nucleotide levels. We confirmed specific spectrum and selected the fingerprint peaks based on the chemical structure of each miRNA and chemical bonding in hybridization. Each fingerprint peak for the target miRNAs was detectable with ultra-high sensitivity (LODs of 3.53 fM, 2.17 fM and 2.16 fM) for the model analytes of the cancer metastasis state, miR–10b, miR–21 and miR–373, respectively. This plasmonic biosensor offers many advantages such as label-free detection, high selectivity, high sensitivity and multiplex detection capability. Taken together, the results show the successful quantification of miRNAs directly from patient-mimicked serum and cancer cell line, proving that this biosensor can be useful in the diagnosis and treatment prognosis of intractable diseases and that it may also be useful for evaluating the therapeutic effects of anticancer drugs in the near future.

Conflicts of interest

There are no conflicts to declare

Acknowledgements

This research was supported by the National Research Foundation of Korea (NRF) grants (Grant No. NRF-2016R1A2A1A05005465/2017R1A5A1070259) and grants (2014M1A8A1049278) from the Korea CCS R & D Center (Korea CCS 2020 Project) grant funded by the Korea government (Ministry of Science and ICT).

References

1 E. Larrea, C. Sole, L. Manterola, I. Goicoechea, M. Armesto, M. Arestin, M. M. Caffarel, A. M. Araujo, M. Araiz, M. Fernandez-Mercado and C. H. Lawrie, *Int. J. Mol. Sci*. 2016, **17**, 627-668, DOI: 10.3390/ijms17050627.
2 R. Visone and C. M. Croce, *Am J Pathol*. 2009, **174**, 1131–1138.
3 H. Dong, J. Lei, L. Ding, Y. Wen, H. Ju, and X. Zhang, *Chem. Rev.* 2013, **113**, 6207−6233. DOI: 10.1021/cr300362f.
4 Z. J. Zhang and S. L. Ma, *Oncol Rep.* 2012, **27**, 903–910. DOI: 10.3892/or.2011.1611.
5 M. Madhavan, K. Cuk, B. Burwinkel and R. Yang, *Front Genet.* 2013, **4**, 116-128. DOI: 10.3389/fgene.2013.00116.
6 M. A. Cortez, C. Bueso–Ramos, J. Ferdin, G. Lopez–Berestein, A. K. Sood, and G. A. Calin, *Nat Rev Clin Oncol.* 2011, **8**, 467–477. DOI: 10.1038/nrclinonc.2011.76.
7 E. E. Creemers, A. J. Tijsen, and Y. M. Pinto, *Circ Res.* 2012, **110,** 483–495. DOI: 10.1161/CIRCRESAHA.111.247452.
8 L. X. Yan, X. F. Huang, Q. Shao, Y. M. Huang, L. Deng, Q. L. Wu, Y. X. Zeng and J. Y. Shao, *RNA.* 2008, **14**, 2348–2360. DOI: 10.1261/rna.1034808.
9 G. J. Zhang, J. H. Chua, R. E. Chee, A. Agarwal, and S. M. Wong, *Biosens Bioelectron.* 2009, **24**, 2504–2508. DOI: 10.1016/j.bios.2008.12.035.
10 W. T. Wang and Y. Q. Chen, *J Hematol Oncol.* 2014, **7**, 86-94. DOI: 10.1186/s13045-014-0086-0.
11 A. H. Nguyen, J. U. Lee and S. J. Sim, *J. Opt.* 2015, **17,** 114022. DOI:10.1088/2040-8978/17/11/114022.
12 K. A. Willets, *Anal Bioanal Chem.* 2009, **394**, 85-94. DOI: 10.1007/s00216-009-2682-3.
13 Y. T. Kim, J. Schilling, S. L. Schweizer, G. Sauer, R. B. Wehrspohn *Photonics and Nanostructures – Fundamentals and Applications.* 2017, **25**, 65–71
14 L. Ma, J. Teruya-Feldstein and R. A. Weinberg, *Nature.* 2007, **449**, 682–688.
15 Q. Huang, K. Gumireddy, M. Schrier, C. Le Sage, R. Nagel, S. Nair, D. A. Egan, A. Li, G. H. Huang, A. J. Klein-Szanto, P. A. Gimotty, D. Katsaros, G. Coukos, L. Zhang, E. Puré and R. Agami, *Nat Cell Biol.* 2008, **10**, 202–210. DOI: 10.1038/ncb1681.
16 S. L. Kleinman, R. R. Frontiera, A. Henry, J. A. Dieringer and R. P. Van Duyne, *Phys Chem Chem Phys.* 2013, **15**, 21-36. DOI: 10.1039/c2cp42598j.
17 J. Tang, F. S. Ou, H. P. Kuo, M. Hu, W. F. Stickle, Z. Li and R. S. Williams, *Appl Phys A.* 2009, **96**, 793–797. DOI: 10.1007/s00339-009-5305-0.
18 L. G. Carrascosa, L. Martınez, Y. Huttel, E. Roman, L. M. Lechuga, *Eur Biophys J.* 2010, **39**, 1433–1444. DOI: 10.1007/s00249-010-0599-6
19 H. Jansen, M. de Boer, R. Legtenberg and M. Elwenspoek, *J. micromech microengin.* 1995, **5**, 115–120.
20 E. D. Diebold, N. H. Mack, S. K. Doorn, and E. Mazur, *Langmuir.* 2009, **25**, 1790–1794. DOI: 10.1021/la803357q.
21 M. S. Schmidt, J. Hübner, A. Boisen, *Adv. Opt. Mat.* 2012, **24** OP11-OP18.
22 A. H. Nguyen, J. U. Lee and S. J. Sim, *Nanoscale.* 2016, **8**, 4599–4607. DOI: 10.1039/c5nr08098c
23 S. Song, A. H. Nguyen, J. U. Lee, M. Cha and S. J. Sim, *Analyst*. 2016, **141**, 2493–2501. DOI: 10.1039/c5an02397a.
24 J. U. Lee, A. H. Nguyen, and S. J. Sim, *Biosens Bioelectron.* 2015, **74**, 341–346. DOI: 10.1016/j.bios.2015.06.059.
25 A. H. Nguyen, J. W. Lee, H. I. Choi, H. S. Kwak and S. J. Sim, *Biosens Bioelectron.* 2015, **70**, 358–365. DOI: 10.1016/j.bios.2015.03.064. nano gap
26 C. L. Wong, U. S. Dinish, M. S. Schmidt, M. Olivo, *Analytica Chimica Acta.* 2014, **844**, 54-60.
27 J. Li, C. Wei, W. Ma, Q. An, J. Guo, J. Hu, and C. Wang, *J. Mater. Chem.* 2012, **22**, 12100

View Article Online
DOI: 10.1039/C8AN01745J

28 T. Kang, H. Kim, J. M. Lee, H. Lee, Y. S. Choi, G. Kang, M. K. Seo, B. H. Chung, Y. Jung, B. Kim, *Small* 2014, **10**, 4200-4206
29 C. Novara, A. Chiadò, N. Paccotti, S. Catuogno, C. L. Esposito, G. Condorelli, V. De Franciscis, F. Geobaldo, P. Rivolo, F. Giorgis, *Faraday discussions.* 2017, **205**, 271-289.
30 X. Tan, J. Melkersson, S. Wu, L. Wang, and J. Zhang, *Chemphyschem.* 2016, **17**, 2630–2639. DOI: 10.1002/cphc.201600286.
31 J. L. Abell, J. M. Garren, J. D. Driskell, R. A. Tripp, and Y. Zhao, *J. Am. Chem. Soc.* 2012, **134**, 12889−12892. DOI: 10.1021/ja3043432.
32 N. H. Jung, *Bull. Korean Chem. Soc.* 2002, **23**, 1790–1800.
33 L. J. Xu, Z. C. Lei, J. Li, C. Zong, C. J. Yang, and B. Ren, *J. Am. Chem. Soc.* 2015, **137**, 5149−5154. DOI: 10.1021/jacs.5b01426.
34 G. J. Puppels, C. Otto, J. Greve, M. Robert-Nicoud, D. J. Arndt-Jovin and T. M. Jovin, *Biochemistry.* 1994, **33** 3386–3395.
35 Y. Lu and Q. Huang, *Anal. Methods.* 2013, **5**, 3927–3932. DOI: 10.1039/C3AY40099A.
36 A. Barhoumi, D. Zhang, F. Tam and N. J. Halas, *J. Am. Chem. Soc.* 2008, **130**, 5523–5529. DOI: 10.1021/ja800023j.
37 A. Barhoumi and N. J. Halas, *J. Am. Chem. Soc.* 2010, **132**, 12792–12793. DOI: 10.1021/ja105678z.
38 E. Prado, N. Daugey, S. Plumet, L. Servant and S. Lecomte, *Chem Commun (Camb).* 2011, **47**, 7425–7427. DOI: 10.1039/c1cc11925g.
39 K. Sun, Q. Huang, G. Meng and Y. Lu, *ACS Appl Mater Interfaces.* 2016, **8**, 5723–5728. DOI: 10.1021/acsami.5b12866.
40 C. V. Pagba, S. M. Lane and S. Wachsmann–Hogiu, *J. Raman Spectrosc.* 2010, **41**, 241–247. DOI: 10.1002/jrs.2428.
41 M. D. Porter, R. J. Lipert, L. M. Siperko, G. Wang and R. Narayanan, *Chem. Soc. Rev.* 2008, **37**, 1001–1011. DOI: 10.1039/b708461g.
42 W. Wang, H. Ouyang, S. Yang, L. Wang and Z. Fu, *Analyst*. 2015, **140,** 1215–1220. DOI: 10.1039/c4an01921k.
43 A. Turchinovich and B. Burwinkel, *RNA Biol.* 2012, **9,** 1066–1075. DOI: 10.4161/rna.21083.
44 D. Tehler, N. M. Høyland-Kroghsbo and A. H. Lund, *RNA Biol.* 2011, **8,** 728-734. DOI: 10.4161/rna.8.5.16324.
45 K. Gracie, E. Correa, S. Mabbott, J. A. Dougan, D. Graham, R. Goodacre and K. Faulds, *Chem. Sci,* 2014, **5**, 1030–1040. DOI: 10.1039/C3SC52875H.
46 M. L. Si, S. Zhu, H. Wu, Z. Lu, F. Wu, Y. Y. Mo. *Oncogene.* 2007, **26**, 2799–2803.